

Submitted, accepted and published by:  
International Journal of Hydrogen Energy 35 (2010) 151-160

## **Hydrogen production by auto-thermal chemical-looping reforming in a pressurized fluidized bed reactor using Ni-based oxygen carriers**

**María Ortiz, Luis F. de Diego\*, Alberto Abad, Francisco García-Labiano, Pilar Gayán, Juan Adánez**

Department of Energy and Environment, Instituto de Carboquímica (C.S.I.C.)

Miguel Luesma Castán 4, 50018 Zaragoza, Spain

Phone number: +34 976 733 977

Fax number: +34 976 733 318

E-mail: [ldediego@icb.csic.es](mailto:ldediego@icb.csic.es)

\*Corresponding Author. Tel.: +34-976-733977; fax: +34-976-733318; E-mail address:

[ldediego@icb.csic.es](mailto:ldediego@icb.csic.es) (L.F. de Diego)

### **Abstract**

This work presents the experimental results obtained during auto-thermal chemical looping reforming (CLRa) in a semicontinuous pressurized fluidized bed reactor working with two Ni-based oxygen carriers and using methane as fuel. During operation the effect of the total pressure, reduction reaction temperature, and oxygen carrier-to-fuel molar ratio on CH<sub>4</sub> conversion, gas outlet concentrations, and carbon formation was analyzed. In the range of pressures analyzed (up to 10 bars), it was found that an increase in the total operating pressure did not produce a negative effect on the gas

product distribution obtained in the process. At all operating pressures the CH<sub>4</sub> conversion was very high (>98%) and no carbon formation was detected. The most important variable affecting the gas product distribution was the solid circulation rate, that is, the oxygen carrier-to-fuel molar ratio (NiO/CH<sub>4</sub>).

The oxygen carriers were physically and chemically characterized by several techniques before and after using in the pressurized fluidized bed reactor. Important changes in the surface texture and the solid structure of the oxygen carrier particles were not detected. These results suggest that these oxygen carriers could have a high durability, being suitable for use in a pressurized CLRa system.

**Keywords:** Hydrogen, Chemical looping, Oxygen carrier, Nickel oxide, Pressurized Fluidized bed

## **1. Introduction**

The stabilization of atmospheric greenhouse gas concentrations can not be reached without the CO<sub>2</sub> capture and storage (CCS). There are different CCS technologies available for the emissions produced in power plants. Some of these technologies are based on H<sub>2</sub> production with CO<sub>2</sub> capture (pre-combustion process). On the other hand, CO<sub>2</sub> capture technology applied to transport sector is more complex, being the use of H<sub>2</sub> as fuel one possible option to reduce the CO<sub>2</sub> emissions.

Hydrogen can be produced from renewable energy sources through water electrolysis, from solid fossil fuels via gasification, or from gaseous fossil fuels via reforming, mainly from natural gas. In this last option, CO<sub>2</sub> is produced as by-product and must be captured and stored to avoid its emission, but today the reforming processes also have advantages as the technology has been practiced for decades and the H<sub>2</sub> cost is less than H<sub>2</sub> produced from renewable energy sources or from solid fossil fuels via gasification.

CO<sub>2</sub> capture technology integrated with H<sub>2</sub> production is available today with its high cost being the main barrier to its use. In the CACHET project the integration of CO<sub>2</sub> capture technologies with H<sub>2</sub> production systems for power generation and fuel applications are being studied (CACHET project, FP6-019972). The overall goal of the CACHET project is to develop innovative technologies which will substantially reduce the cost of CO<sub>2</sub> capture whilst simultaneously producing H<sub>2</sub> from natural gas. Some of the technologies investigated are based on Chemical-Looping Combustion (CLC) process (Rydén and Lyngfelt (2006b), Chiesa et al. (2008)).

CLC is a novel combustion technology with inherent separation of the greenhouse gas CO<sub>2</sub> that involves the use of an oxygen carrier, which transfers oxygen from air to the fuel avoiding the direct contact between them. CLC system is made of two interconnected reactors, designated as air and fuel reactors. In the fuel reactor, the fuel gas (C<sub>n</sub>H<sub>m</sub>) is oxidized to CO<sub>2</sub> and H<sub>2</sub>O by a metal oxide (MeO) that is reduced to a metal (Me) or a reduced form of MeO. The metal or reduced oxide is further transferred into the air reactor where it is oxidized with air, and the material regenerated is ready to start a new cycle. The flue gas leaving the air reactor contains N<sub>2</sub> and unreacted O<sub>2</sub>. The

exit gas from the fuel reactor contains only CO<sub>2</sub> and H<sub>2</sub>O. After water condensation, almost pure CO<sub>2</sub> can be obtained with little energy lost for component separation.

Chemical-Looping auto-thermal Reforming (CLRa) (Mattisson and Lyngfelt, 2001) also uses a metal oxide to transfer oxygen to the fuel (Figure 1), the main difference being that the desired product is syngas (H<sub>2</sub> + CO). In the CLRa process the air to fuel ratio is kept low to prevent the complete oxidation of the fuel to CO<sub>2</sub> and H<sub>2</sub>O. The major advantage of this process is that the heat needed for converting CH<sub>4</sub> to H<sub>2</sub> is supplied without costly oxygen production, without mixing of air with carbon containing fuel gases or without using part of the H<sub>2</sub> produced in the process. An important aspect to be considered in a CLRa system is the heat balance. The oxidation reaction of the metal oxide is very exothermic, however, the reduction reactions are endothermic. So, the heat for the endothermic reduction reactions is given by the circulating solids coming from the air reactor at higher temperature. The heat generated in the air reactor must be high enough to fulfil the heat balance in the system.

A key issue for the CLRa technology development is the selection of an oxygen carrier with suitable properties: enough reactivity through cycles to reduce solids inventory; high resistance to attrition to minimize losses of elutriated solid; complete fuel conversion to CO and H<sub>2</sub>; negligible carbon deposition what would release CO<sub>2</sub> in the air reactor and good properties for fluidization (no presence of agglomeration). In addition, other characteristics such as simple preparation method would be desirable to reduce costs. Fe-, Ni-, Cu-, Ce- and Mn-based oxygen carriers supported on different inert materials, such as Al<sub>2</sub>O<sub>3</sub>, SiO<sub>2</sub>, Mg-ZrO<sub>2</sub> and prepared by different methods, have

been studied to be used in a CLRa system (Zafar et al. (2005), Johansson et al. (2008), de Diego et al. (2008), He et al. (2009)), but Ni-based oxygen carriers appears the most interesting due to its strong catalytic properties. In fact, metallic Ni is used in most commercial steam reforming catalyst's. Rydén et al. (2008b) also tested in a fixed bed reactor  $\text{La}_x\text{Sr}_{1-x}\text{FeO}_{3-\delta}$  perovskites as oxygen carriers for CLRa. They found that perovskites provided very high selectivity towards  $\text{CO}/\text{H}_2$  and should be well suited for CLRa but the long-term chemical and mechanical properties of the perovskite particles are largely unknown.

Atmospheric continuous auto-thermal chemical-looping reforming working with Ni-based oxygen carriers has been demonstrated by Rydén et al. (2006a, 2008a) and by de Diego et al. (2009) in small laboratory units, and by Bolhàr-Nordnkampf et al. (2009) in a  $120 \text{ kW}_{\text{th}}$  pilot plant. Rydén and Lyngfelt (2004) carried out a thermodynamic analysis to investigate the characteristics of some processes that utilize chemical-looping technology for production of  $\text{H}_2$ . These authors found that the atmospheric processes have large  $\text{H}_2$  production but the electricity needed to compress the product is considerable, and concluded that a pressurized CLRa system is less straightforward but would have potential to achieve much higher overall efficiency. Siriwardane et al. (2007) and García-Labiano et al. (2006) studied, in a packed reactor and in a thermogravimetric analyzer (TGA), the effect of the pressure on the behaviour of several oxygen carriers for CLC. In both works it was showed that the pressure had a positive effect on the reaction rates, although the reactivity increase was not as high as expected. There are no studies in the literature about the effect of the operating pressure in a CLRa system. So, it is needed to study this effect working with continuous units.

In this work the effect of total pressure on CH<sub>4</sub> conversion, gas outlet concentrations, and carbon formation was studied in a semicontinuous pressurized fluidized bed reactor working with two Ni-based oxygen carriers. The effect of different operating variables, like reduction reaction temperature and oxygen carrier to fuel ratio (NiO/CH<sub>4</sub>), was also analyzed at pressures up to 10 bars.

## **2. Experimental Section**

### **2.1. Materials**

The behaviour of two oxygen carriers based on nickel was analyzed in this work. In both of them, Al<sub>2</sub>O<sub>3</sub> was selected as support to increase the mechanical strength of the material. NiO21- $\gamma$ Al<sub>2</sub>O<sub>3</sub> was prepared by incipient wetness impregnation over commercial  $\gamma$ Al<sub>2</sub>O<sub>3</sub> (Puralox NWa-155, Sasol Germany GmbH) and NiO18- $\alpha$ Al<sub>2</sub>O<sub>3</sub> was prepared by incipient wetness impregnation over  $\alpha$ Al<sub>2</sub>O<sub>3</sub> (obtained by calcination of  $\gamma$ Al<sub>2</sub>O<sub>3</sub> at 1150 °C during 2 hours). The details of the preparation of both oxygen carriers have been described elsewhere (Gayán et al. (2008)). The oxygen carriers are designated with the metal oxide followed by its weight content and the inert used as support.

### **2.2. Oxygen carrier characterization**

The oxygen carriers were physically and chemically characterized by several techniques. The bulk density of the oxygen carrier particles was calculated weighting a known volume of solid and assuming that the void was 0.45 corresponding to loosely packed bed. The force needed to fracture a particle was determined using a Shimpo FGN-5X crushing strength apparatus. The mechanical strength was taken as the average value of at least 20 measurements. The porosity was measured by Hg intrusion in a Quantachrome PoreMaster 33. The identification of crystalline chemical species was carried out by powder X-ray diffraction (XRD) patterns acquired in an X-ray diffractometer Bruker AXS D8ADVANCE using Ni-filtered Cu K $\alpha$  radiation equipped with a graphite monochromator. The oxygen carriers were also analyzed in a scanning electron microscope (SEM) ISI DS-130 coupled to an ultra thin window PGT Prism detector for energy-dispersive X-ray (EDX) analysis.

### **2.3. Thermodynamic calculations**

Thermodynamic calculations about the effect of total pressure in a CLRa system were carried out using HSC Chemistry 6.1 (2008) software. The program obtains the equilibrium gas composition by using the method of minimization of the Gibbs free energy of the system. The effect of pressure was analyzed in the range of 1 to 25 bars for a reaction temperature of 900°C, a H<sub>2</sub>O/CH<sub>4</sub> molar ratio of 0.3 and an oxygen carrier to fuel ratio (NiO/CH<sub>4</sub>) of 1.25, which is the optimum value for the fulfilment of the heat balance in a CLRa process (de Diego et al. (2009)).

Figure 2 shows the results of the thermodynamic calculation. It can be observed that the thermodynamic equilibrium for the reforming reactions is less favourable to the production of syngas ( $\text{CO} + \text{H}_2$ ) at elevated pressure. An increase in the operating pressure produced a decrease in the  $\text{CH}_4$  conversion, an increase in the  $\text{CO}_2$  and  $\text{H}_2\text{O}$  concentrations and a decrease in the  $\text{H}_2$  and  $\text{CO}$  concentrations. In this way, to achieve at high pressure the same  $\text{CH}_4$  conversion as at atmospheric pressure an increase in the fuel reactor temperature is needed, as it can be observed in the figure 2.

#### **2.4. Reactivity tests in thermogravimetric analyzer**

Reactivity tests of the oxygen carriers were carried out in an atmospheric thermogravimetric analyzer (TGA), CI Electronics type, described elsewhere (de Diego et al. (2004)). For the experiments, the oxygen carrier was loaded in a platinum basket and heated to the operating temperature ( $900^\circ\text{C}$ ) in air atmosphere. After weight stabilization, the experiment was started by exposing the oxygen carrier to alternating reducing and oxidizing conditions. The reducing gas was saturated in water by bubbling it through a water containing saturator at the selected temperature to reach the desired water concentration. The gas selected for the reducing experiments was composed by 15 vol.%  $\text{CH}_4$ , and 20 vol.%  $\text{H}_2\text{O}$  ( $\text{N}_2$  balance) and the gas used for oxidation was 100 vol.% air. To avoid mixing of combustible gas and air, nitrogen was introduced for 2 min after each reducing and oxidizing period.

#### **2.5. Experimental Facility**



A semicontinuous fluidized bed reactor was built to analyze the effect of the total pressure on the H<sub>2</sub> yield, selectivity, carbon formation, gas outlet concentrations and oxygen carrier integrity, in a CLRa process. Figure 3 shows the schematic diagram of the experimental setup, which was basically composed of a system for gas feeding, a continuous system for solids feeding, a pressurized reactor and a gas analysis system. The gas feeding system (1) had different mass flow controllers for different gases and water. The fluidized bed, with a bed height of 0.15 m, was placed inside a Kanthal reactor of 0.038 m D.I. and 0.58 m height (2), with a preheating zone just under the distributor. The reactor was inside an electrically heated furnace (3). A pressure valve (9) located at the gas exit line controlled the reactor pressure. There was a hot filter (8) downstream from the fluidized bed reactor to recover the solids elutriated from the bed. Both gas feeding line and gas exit line were heated to avoid water condensation.

The oxygen carrier was fed to the reactor from a heated lock hopper (4), located in the upper part of the system, using a screw feeder (5). The flow rate of solids entering the reactor was controlled by regulating the velocity (6) of the screw feeder. The reacted oxygen carrier overflowed into a collecting hopper (7) keeping constant the solid inventory in the system. Different gas analyzers continuously measured the gas composition at each time. The CO, CO<sub>2</sub>, H<sub>2</sub>O, and CH<sub>4</sub> gas concentrations were measured in FTIR (Fourier transform infrared spectroscopy) and NDIR (non dispersive infrared sensor) analyzers, the O<sub>2</sub> concentration was measured in a paramagnetic analyzer, and the H<sub>2</sub> concentration was measured by thermal conductivity.

After construction of the prototype, initial tests of solids feeding were carried out to learn about the control of the system. In those first tests, the mass balances showed very high water content at the gas outlet stream because the oxygen carriers adsorbed water during handling (Figure 4). To avoid this problem, it was necessary to dry the oxygen carriers before feeding to the reactor. For that, it was set up a furnace (3) around the solid feed hopper, and the solid was dried flowing  $N_2$  through it. This allowed to keep the oxygen carrier hot and free of water. As can be seen in the test showed in Figure 4, after drying the solid, no  $H_2O$  concentration was measured along the test. Only a small  $H_2O$  concentration coming from the solid that was in the screwfeeder, which was not well dried, was measured at the beginning of the test.

## **2.6. Experimental procedure**

The experimental facility used in this work was a semicontinuous system. So, the experiments were divided in two tests, the reduction test and the oxidation test. Figure 5 shows a typical reduction test in the semicontinuous fluidized bed for the  $NiO_{21}-\gamma Al_2O_3$  oxygen carrier at an operating pressure of 5 bars. During the reduction test, the oxidized oxygen carrier was loaded in the solid feed hopper and, after drying, the whole system was locked and pressurized in nitrogen atmosphere until the desired pressure. Then, the steam was fed to the reactor and after flow stabilization, the oxygen carrier and  $CH_4$  were fed to start the reduction test. The steady-state was reached after 20-40 minutes depending of the operating conditions, and it was maintained for at least 60 minutes. The reduced oxygen carrier overflowed into the solid collecting hopper. When the reduction test was finished, the system was depressurized and the oxygen carrier was

recovered. The oxidation of the oxygen carrier was carried out at atmospheric pressure in a similar way.

### **3. Results and discussion**

Reforming tests under different operation conditions were conducted in the facility with the two oxygen carriers using CH<sub>4</sub> as fuel. The selected range of operating conditions (with the exception of the solid feeding rate) was the same for the two oxygen carriers. The effect of the total pressure was studied in the range of 1-10 bars. To analyze the effect of the total pressure for a constant gas velocity and NiO/CH<sub>4</sub> molar ratio, two kinds of experiments can be carried out. The first option is to perform experiments with a constant concentration of CH<sub>4</sub> at the different total pressures. This involves an increase in the CH<sub>4</sub> flow rate with increasing the pressure. For a constant NiO/CH<sub>4</sub> molar ratio an increase in the CH<sub>4</sub> flow rate produces an increase in the oxygen carrier feed flow rate and as a consequence a decrease in the mean residence time of the oxygen carrier in the fluidized bed reactor. The second option is to perform experiments with a constant CH<sub>4</sub> partial pressure at the different total pressures. In this case, the CH<sub>4</sub> concentration decreases with increasing the pressure but the CH<sub>4</sub> flow rate is kept constant at the different total pressures. So, the solid feed flow rate and the mean residence time of the oxygen carrier in the fluidized bed reactor are kept constants for the same NiO/CH<sub>4</sub> molar ratio at different total pressures.

In this work, the second option was used to carry out the experimental tests. The reduction tests were carried out with a CH<sub>4</sub> partial pressure of 0.5 bars (38.2 NI/h), an

inlet superficial gas velocity into the reactor of 0.08 m/s, and a H<sub>2</sub>O/CH<sub>4</sub> molar ratio of 0.3. Table 1 shows the CH<sub>4</sub> concentrations used at the different total pressures.

To study the effect of the reduction reaction temperature at different operating pressures, the temperature in the reactor was varied over a range of 800-900 °C. The effect of oxygen carrier to fuel ratio (NiO/CH<sub>4</sub>) on the CH<sub>4</sub> conversion and gas product distribution was analyzed by controlling the solid feeding flow rate by means of the velocity of the screw feeder, and took values from 0.8 to 2.6 kg/h. The mean residence time of solids varied from 3 to 9 min for NiO21- $\gamma$ -Al<sub>2</sub>O<sub>3</sub> and from 4 to 13 min for NiO18- $\alpha$ -Al<sub>2</sub>O<sub>3</sub> as a function of the NiO/CH<sub>4</sub> molar ratio used.

The oxidation of the oxygen carrier was carried out at atmospheric pressure and a temperature of 950°C with an inlet superficial gas velocity into the reactor of 0.08 m/s and a gas composition of 15 vol% O<sub>2</sub> in N<sub>2</sub>.

The steady-state for the different operating conditions was maintained for at least 1 hour in each test. A total of more than 50 hours of operation with each oxygen carrier, taking into account only the reduction tests, were carried out.

### **3.1. Evaluation of the data**

The gas product concentrations were measured by on line analyzers. The main reactions happening with different contribution in the reactor during the oxygen carrier reduction test are:

*Oxidation*



*Partial oxidation*



*Steam reforming catalyzed by Ni*



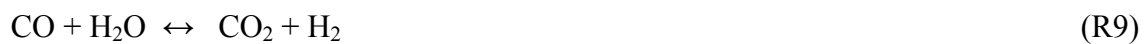
*Methane decomposition catalyzed by Ni*



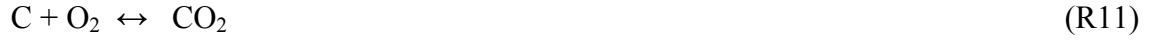
*Carbon gasification*



*Water gas shift*



And during the oxidation test:



Taking into account these reactions, the conversions of the oxygen carriers during the reduction and oxidation periods were calculated from the gas outlet concentrations by the equations:

### *Reduction*

$$X_{red} = \frac{Q_{out}}{n_0 P_{tot}} (2P_{CO_2,out} + P_{CO,out} + P_{H_2O,out}) \quad (1)$$

$$Q_{out} = Q_{in} \left( \frac{P_{N_2,in}}{P_{N_2,out}} \right) = Q_{in} \left( \frac{P_{N_2,in}}{(1 - P_{CH_4,out} - P_{CO_2,out} - P_{CO,out} - P_{H_2,out} - P_{H_2O,out})} \right) \quad (2)$$

### *Oxidation*

$$X_{oxi} = \frac{2Q_{out}}{n_0 P_{tot}} \left( \frac{Q_{in}}{Q_{out}} P_{O_2,in} - P_{O_2,out} - 1/2 P_{CO,out} - P_{CO_2,out} \right) \quad (3)$$

$$Q_{out} = \frac{Q_{in} (1 - P_{O_2,in})}{(1 - P_{CO_2,out} - P_{CO,out} - P_{O_2,out})} \quad (4)$$

where  $X$  is the conversion of the oxygen carrier,  $Q_{in}$  is the molar flow of the gas coming into the reactor,  $Q_{out}$  is the molar flow of the gas leaving the reactor,  $P_{tot}$  is the total pressure,  $P_{i,in}$  is the partial pressure of gas  $i$  coming into the reactor,  $P_{i,out}$  is the partial pressure of gas  $i$  exiting the reactor,  $n_0$  are the moles of oxygen which can be removed from fully oxidized oxygen carrier. The last terms in equation 3 take into account the formation of CO and CO<sub>2</sub> during the oxidation test due to the oxidation of C (reactions R11 and R12) coming from the decomposition of CH<sub>4</sub> (reaction R6).

For better comparison, the results showed in this work are presented in N<sub>2</sub> free basis and/or dry N<sub>2</sub> free basis.

### **3.2. Effect of Total Pressure**

The effect of the total pressure was studied in the range of 1-10 bars. Under all operating conditions, the inlet molar flow of methane was maintained constant. Figure 6 shows the effect of the total pressure on the gas product concentrations for both oxygen carriers working at 900°C and a NiO/CH<sub>4</sub> molar ratio of 3.2 for the NiO21- $\gamma$ Al<sub>2</sub>O<sub>3</sub> oxygen carrier and 2.2 for the NiO18- $\alpha$ Al<sub>2</sub>O<sub>3</sub> oxygen carrier. As it can be observed in the figure, the CH<sub>4</sub> conversion was very high in all the range of pressures tested and an increase in the operating pressure did not produce any important change in the gas product distribution of the CLRa process for both oxygen carriers.

The oxygen carrier conversions reached during the reduction reaction were calculated with the equations 1 and 2. It was found that the conversions reached by each oxygen

carrier were very similar at all operating pressures, about 55% for the NiO21- $\gamma$ Al<sub>2</sub>O<sub>3</sub> oxygen carrier and about 80% for the NiO18- $\alpha$ Al<sub>2</sub>O<sub>3</sub> oxygen carrier. The conversions reached by the NiO18- $\alpha$ Al<sub>2</sub>O<sub>3</sub> oxygen carrier were higher than the conversions reached by the NiO21- $\gamma$ Al<sub>2</sub>O<sub>3</sub> oxygen carrier because of its higher reactivity, in good agreement with the reactivity observed in the TGA. Figure 7 shows the reduction reactivity measured in the TGA for both oxygen carriers using as reacting gases 15 vol.% CH<sub>4</sub> and 20 vol.% H<sub>2</sub>O (N<sub>2</sub> balance). As it can be seen, the NiO18- $\alpha$ Al<sub>2</sub>O<sub>3</sub> oxygen carrier showed higher reactivity than the NiO21- $\gamma$ Al<sub>2</sub>O<sub>3</sub> oxygen carrier during the reduction reaction. The low reduction reactivity of the oxygen carrier of NiO on  $\gamma$ Al<sub>2</sub>O<sub>3</sub> was due to the solid state reaction between the NiO and the  $\gamma$ Al<sub>2</sub>O<sub>3</sub> to form NiAl<sub>2</sub>O<sub>4</sub>, as it is shown in the XRD patterns (see Table 2). It must be taken into account that the reaction rate of CH<sub>4</sub> with NiAl<sub>2</sub>O<sub>4</sub> is lower than with free NiO (de Diego et al. (2008)). On the contrary, the high reactivity of the carrier of NiO on  $\alpha$ Al<sub>2</sub>O<sub>3</sub> was because the interaction between the NiO and the support was reduced using the  $\alpha$ Al<sub>2</sub>O<sub>3</sub>. As can be seen in Table 2, free NiO was observed in this oxygen carrier.

Taking into account the conversions reached by both oxygen carriers for the operating conditions used in Figure 6 (a temperature of 900°C and a NiO/CH<sub>4</sub> molar ratio of 3.2 for the NiO21- $\gamma$ Al<sub>2</sub>O<sub>3</sub> oxygen carrier and 2.2 for the NiO18- $\alpha$ Al<sub>2</sub>O<sub>3</sub> oxygen carrier), the NiO<sub>reacted</sub>/CH<sub>4</sub> molar ratio was 1.8 for both oxygen carriers. Figure 8 shows the gas product compositions at different operating pressures given by the thermodynamic equilibrium for a NiO<sub>reacted</sub>/CH<sub>4</sub> molar ratio of 1.8, and the experimental gas compositions obtained working with both oxygen carriers. It can be observed very similar gas compositions working at the same NiO<sub>reacted</sub>/CH<sub>4</sub> molar ratio with both



oxygen carriers at all operating pressures. In addition, it was found that these gas product compositions were close to thermodynamic equilibrium.

An important obstacle in a pressurized CLRa process could possibly be the carbon formation because the reactions R11-R12 are favoured at elevated pressures. However, no carbon formation was detected at all operating pressures tested.

### **3.3. Effect of Reduction Reaction Temperature**

From a thermodynamic point of view, the reduction reaction temperature at elevated pressure must be higher than at atmospheric pressure to achieve the same CH<sub>4</sub> conversion. So, it is important to analyze the effect of the reduction reaction temperature on the gas product compositions at elevated pressures. The effect of reduction reaction temperature was tested in the range of 800-900°C. At all reduction reaction temperatures, the inlet molar flow of methane was maintained constant. Figure 9 shows the effect of reduction reaction temperature on the gas product compositions at operating pressures of 1 and 10 bars for the oxygen carrier NiO18- $\alpha$ Al<sub>2</sub>O<sub>3</sub>. It can be observed the same effect of the reduction reaction temperature on the gas product composition at both operating pressures. The CH<sub>4</sub> conversion was very high (>98%) in the range of temperature tested, and for the same oxygen carrier-to-fuel ratio, an increase in the reduction reaction temperature produced a small increase in the CH<sub>4</sub> conversion, a slight increase in the CO<sub>2</sub> and H<sub>2</sub>O concentrations and a slight decrease in the H<sub>2</sub> and CO concentrations. The increase in the CH<sub>4</sub> conversion with an increase in the reduction reaction temperature could be due to the increase of R1, R4, and R5

reaction rates, and the increase in the CO<sub>2</sub> and H<sub>2</sub>O concentrations and decrease in the H<sub>2</sub> and CO concentrations due to the increase of R1, R2, and R3 reaction rates. It must be taken into account that an increase in the reduction reaction temperature increased the oxygen carrier conversion and as a consequence more oxygen was available for oxidation.

### **3.4. Effect of Oxygen Carrier-to-Fuel Ratio**

As it was previously commented, in the CLRa process the metal oxide is used to transfer oxygen to the fuel. In addition, because the oxidation reaction of the metal oxide is very exothermic and the reduction reactions are endothermic, the heat for the endothermic reduction reactions is given by the circulating solids coming from the air reactor at higher temperature. The heat generated in the air reactor must be high enough to fulfil the heat balance in the system. So, a basic operating variable for the CLRa process is the oxygen carrier-to-fuel molar ratio which, for a given fuel flow rate fed to the reactor, depends on the solid feeding flow rate. In this experimental setup the solid feeding flow rates were controlled by means of the velocity of the screw feeder, and took values from 0.8 to 2.6 kg/h.

Figures 10 and 11 show the effect of oxygen carrier-to-fuel ratio on the gas product composition for both oxygen carriers working at different pressures and at a temperature of 900 °C. It can be observed that at all operating pressures the gas product distributions obtained working with both oxygen carriers were similar. As expected, it was found that an increase in the oxygen carrier-to-fuel ratio produced an increase in the CO<sub>2</sub> and H<sub>2</sub>O

concentrations and a decrease in the H<sub>2</sub>, CO and CH<sub>4</sub> concentrations at all operating pressures. This was obviously due to the different contribution of the different reactions (R1 to R9) to the overall global process, but specially increasing the oxygen carrier circulation flow rate increased the contribution of the oxidation reactions (reactions R1-R3). Finally, it can be seen in these figures that the gas product compositions were close to thermodynamic equilibrium.

### **3.5. Behaviour of the oxygen carrier particles**

The oxygen carriers were physically and chemically characterized before and after operation in the pressurized fluidized bed reactor. Table 2 shows the main properties of the oxygen carriers. As can be seen, no important changes in the density, porosity, and mechanical strength were observed in the oxygen carrier particles after being used under pressurized conditions. The BET surface area of the NiO<sub>21</sub>- $\gamma$ -Al<sub>2</sub>O<sub>3</sub> oxygen carrier decreased, suggesting that some accumulative thermal sintering was occurring in the oxygen carrier particles along the time during operation in the prototype. However, this thermal sintering did not deactivate the oxygen carrier reactivity. Figure 7 shows the reactivities measured in the TGA for the fresh and used oxygen carriers. The reduction reactivity of the NiO<sub>18</sub>- $\alpha$ -Al<sub>2</sub>O<sub>3</sub> oxygen carrier were hardly affected by the operation, however, the reduction reactivity of NiO<sub>21</sub>- $\gamma$ -Al<sub>2</sub>O<sub>3</sub> oxygen carrier was higher in the used particles. The powder XRD patterns of the used oxygen carriers revealed no new crystalline phases for both oxygen carriers. In addition, the oxygen carrier particles never showed agglomeration or defluidization problems.

The surface texture and the solid structure of the oxygen carriers were analyzed by SEM-EDX. Figure 12 shows the pictures of the oxygen carrier particles, both fresh and used under pressurized conditions. No major differences can be observed between them. The nickel distribution inside the particles was analyzed by EDX in some particles embedded in resin epoxy, cut, and polished. In both oxygen carriers, the Ni was uniformly distributed through the particles and there was not evidence of redistribution or migration of Ni sites during the redox cycles.

The behaviour of the oxygen carriers at high pressure was very similar to that the observed by these oxygen carriers working for more than 50 h operation at atmospheric pressure in a 900 Wth continuous circulating fluidized bed reactor using CH<sub>4</sub> as fuel (de Diego et al. (2009)). So, it can be concluded that the pressure did not produce any negative effect in the behaviour of the oxygen carrier particles. These results suggest that these oxygen carriers could have a high durability, being suitable oxygen carriers for a pressurized CLRa system.

#### **4. Conclusions**

Two Ni-based oxygen carriers, NiO21- $\gamma$ Al<sub>2</sub>O<sub>3</sub> and NiO18- $\alpha$ Al<sub>2</sub>O<sub>3</sub>, prepared by incipient wetness impregnation, have been tested in a semicontinuous pressurized fluidized bed reactor to analyze the effect of the total pressure on the CLRa process. During operation the effect of different operating variables, like reduction reaction temperature and oxygen carrier-to-fuel molar ratio, on CH<sub>4</sub> conversion and gas product distribution was analyzed at pressures up to 10 bars.

It was observed that in all operating pressures tested the CH<sub>4</sub> conversion was very high (>98%) for both oxygen carriers. An increase in the operating pressure did not produce any important change in the gas product distribution of the CLRa process and no carbon formation was detected.

At all operating pressures, an increase in the reduction reaction temperature produced a slight increase in the CH<sub>4</sub> conversion and CO<sub>2</sub> and H<sub>2</sub>O concentrations and a slight decrease in the H<sub>2</sub> and CO concentrations.

An increase in the oxygen carrier-to-fuel ratio produced an increase in the CO<sub>2</sub> and H<sub>2</sub>O concentrations and a decrease in the H<sub>2</sub>, CO and CH<sub>4</sub> concentrations, very similar at all operating pressures. The measured gas concentrations were near to that given by the thermodynamic equilibrium.

Important changes in the surface texture and the solid structure of the oxygen carrier particles were not detected after operation in the semicontinuous pressurized fluidized bed reactor. In addition, the oxygen carriers did not show agglomeration or defluidization problems. These results suggest that these oxygen carriers could have a high durability, being suitable as oxygen carriers for a pressurized CLRa system.

## **Acknowledgments**

This work was partially supported by the European Commission, under the 6th Framework Programme (CACHET Project, Contract no. 019972), from the CCP2 (CO<sub>2</sub> Capture Project), a partnership of BP, Chevron, Conoco-Phillips, Eni Technology, Norsk Hydro, Shell, Suncor, and Petrobras and from the Spanish Ministry of Science and Innovation (CTQ2007-64400). M. Ortiz thanks Diputación General de Aragón for the F.P.I. fellowship.

## References

Bolhàr-Nordenkamp, J., Pröll, T., Kolbitsch, P., Hofbauer, H., 2009. Performance of a NiO-based oxygen carrier for chemical looping combustion and reforming in a 120 kW unit. *Energy Procedia*. 1, 19-25.

Carbon Dioxide Capture and Hydrogen Production from Gaseous Fuels (CACHET project). FP6-019972.

Chiesa, P., Lozza, G., Malandrino, A., Romano, M., Piccolo, V., 2008. Three-reactors chemical looping process for hydrogen production. *Int. J. Hydrogen Energy*. 33, 2233-224.

de Diego, L.F., García-Labiano, F., Adánez, J., Gayán, P., Abad, A., Corbella, B.M., Palacios, J.M., 2004. Development of Cu-based oxygen carriers for chemical-looping combustion. *Fuel*. 83, 1749-1757.

de Diego, L.F., Ortiz, M., Adánez, J., García-Labiano, F., Abad, A., Gayán, P., 2008. Synthesis gas generation by chemical-looping reforming in a batch fluidized bed reactor using Ni-based oxygen carriers. *Chem. Eng. J.* 144, 289-298.

de Diego, L.F., Ortiz, M., Adánez, J., García-Labiano, F., Abad, A., Gayán, P., 2009. Hydrogen production by chemical-looping reforming in a circulating fluidized bed reactor using Ni-based oxygen carriers. *J. Power Sources.* 192, 27-34.

He, F., Wei, Y., Li, H., Wang, H., 2009. Synthesis Gas Generation by Chemical-Looping Reforming Using a Ce-Based Oxygen Carriers modified with Fe, Cu, and Mn Oxides. *Energy Fuels.* 23, 2095-2102.

HSC Chemistry 6.1, 2008. Chemical Reaction and Equilibrium Software with Thermochemical Database and Simulation Module; Outotec Research Oy, Pori, Finland.

García-Labiano, F., Adánez, J., de Diego, L.F., Gayán, P., Abad, A., 2006. Effect of pressure on the behaviour of copper-, iron-, and nickel-based oxygen carriers for chemical-looping combustion. *Energy Fuels.* 20, 26-33.

Gayán, P., de Diego, L.F., García-Labiano, F., Adánez, J., Abad, A., Dueso, C., 2008. Effect of support on reactivity and selectivity of Ni-based oxygen carriers for chemical-looping combustion. *Fuel.* 87, 2641–2650.

Johansson, M., Mattisson, T., Lyngfelt, A., Abad, A., 2008. Using continuous and pulse experiments to compare two promising nickel-based oxygen carriers for use in chemical-looping technologies. *Fuel*. 87, 988-1001.

Mattisson, T., Lyngfelt, A., 2001. Proceedings of the 2nd Nordic Minisymposium on Carbon Dioxide Capture and Storage, Göteborg, Sweden.

Rydén, M., Lyngfelt, A., 2004. Hydrogen and power production with integrated carbon dioxide capture by chemical-looping reforming. Proceedings of the 7<sup>th</sup> International Conference on Greenhouse Gas Control Technologies, Vancouver, Canada.

Rydén, M., Lyngfelt, A., Mattisson, T., 2006. Synthesis gas generation by chemical-looping reforming in a continuously operating laboratory reactor. *Fuel*. 85, 631-1641.

Rydén, M., Lyngfelt, A., 2006. Using steam reforming to produce hydrogen with carbon dioxide capture by chemical-looping combustion. *Int. J. Hydrogen Energy*. 31, 1271-1283.

Rydén, M., Lyngfelt, A., Mattisson, T., 2008. Chemical-looping combustion and chemical-looping reforming in a circulating fluidized-bed reactor using Ni-based oxygen carriers. *Energy Fuels*. 22, 2585-2597.

Rydén, M., Lyngfelt, A., Mattisson, T., Chen, D., Holmen, A., Bjørgum, E., 2008. Novel oxygen-carrier materials for chemical-looping combustion and chemical-looping



reforming;  $\text{La}_x\text{Sr}_{1-x}\text{Fe}_y\text{Co}_{1-y}\text{O}_{3-\delta}$  perovskites and mixed-metal oxides of NiO,  $\text{Fe}_2\text{O}_3$  and  $\text{Mn}_3\text{O}_4$ . *Int. J. Greenhouse Gas Control.* 2, 21-36.

Siriwardane, R., Poston, J., Chaudhari, K., Simonyi, T., Robinson, C., 2007. Chemical-looping combustion of simulated synthesis gas using nickel oxide oxygen carrier supported on bentonite. *Energy Fuels.* 21, 1582-91.

Zafar, Q., Mattisson, T., Gevert, B., 2005. Integrated hydrogen and power production with  $\text{CO}_2$  capture using chemical-looping reforming-redox reactivity of particles of CuO,  $\text{Mn}_2\text{O}_3$ , NiO, and  $\text{Fe}_2\text{O}_3$  using  $\text{SiO}_2$  as a support. *Ind. Eng. Chem. Res.* 44, 3485-3498.

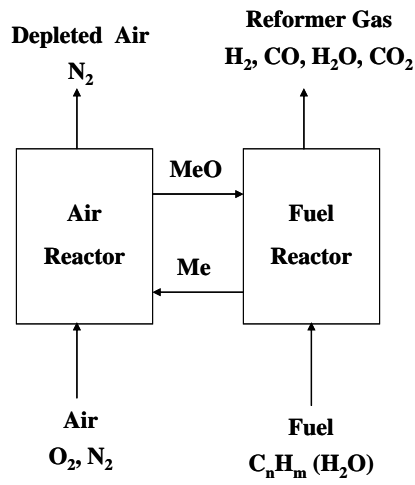


**Figure 1:** Chemical-Looping Reforming.

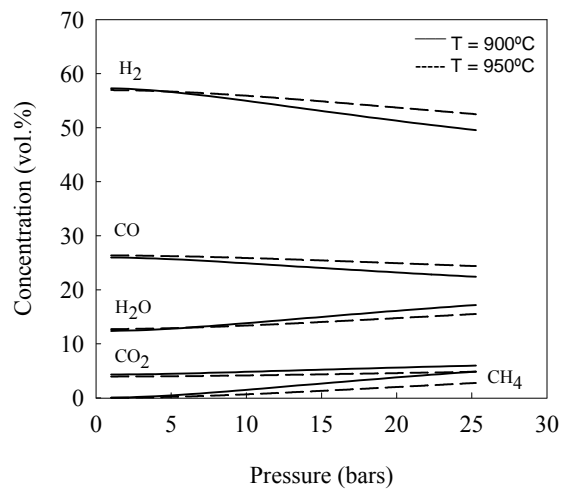


**Figure 2:** Thermodynamic equilibrium gas composition for different operating pressures and temperatures.

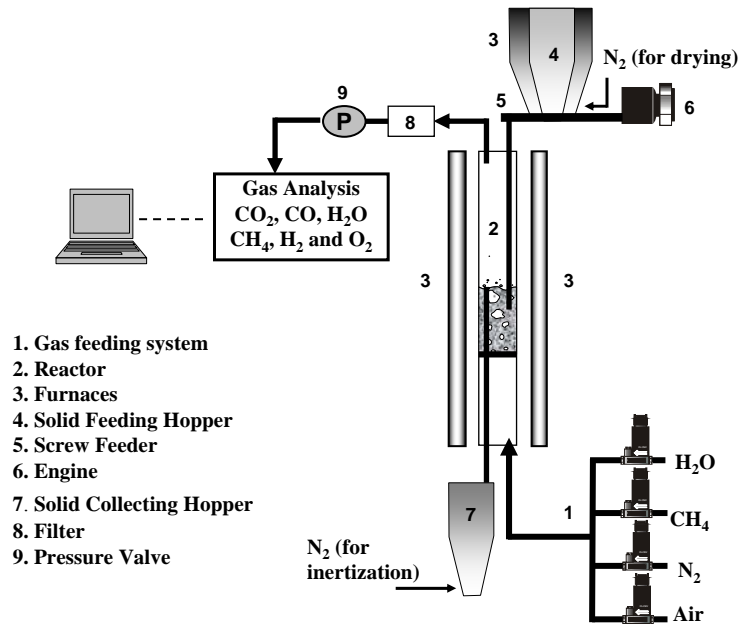


**Figure 3:** Schematic diagram of the semicontinuous pressurized fluidized bed facility for CLRa

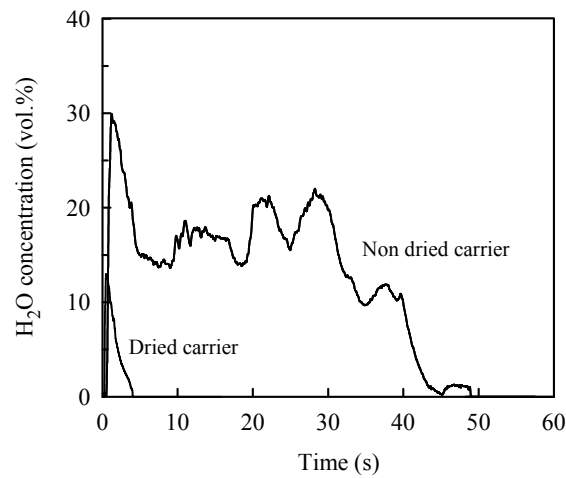


**Figure 4:**  $\text{H}_2\text{O}$  concentration in the gas outlet stream before and after installation of the furnace around the solid feed hopper. Fluidizing gas:  $\text{N}_2$ .  $T = 900^\circ\text{C}$

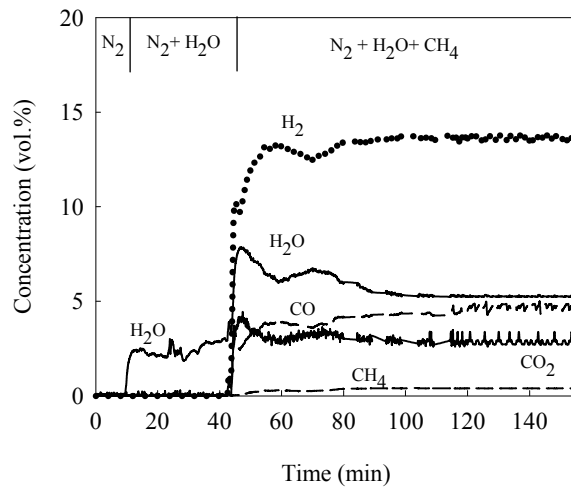


**Figure 5:** Typical reduction test in the semicontinuous fluidized bed facility.

NiO21- $\gamma$ Al<sub>2</sub>O<sub>3</sub>, P = 5 bars, T= 900°C

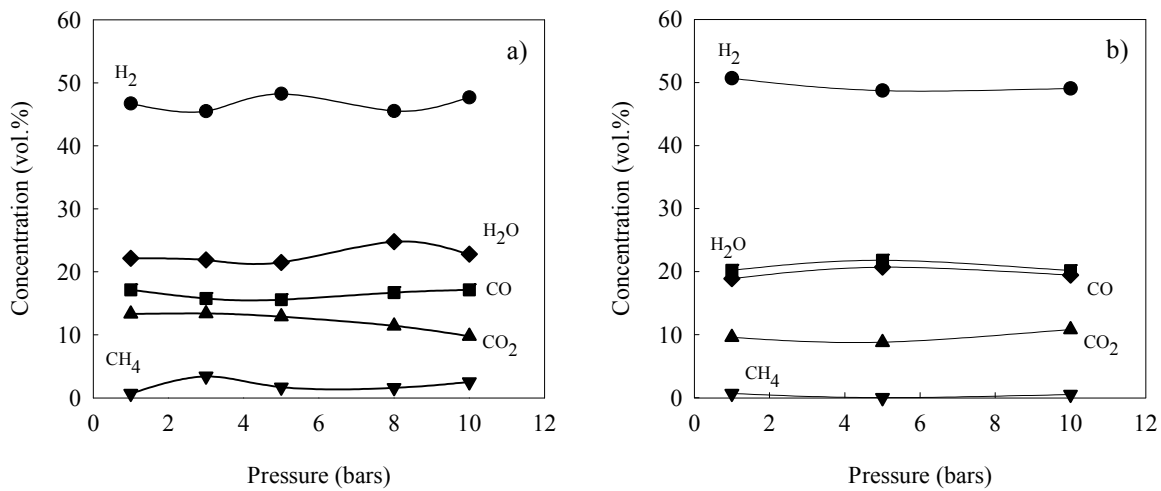


**Figure 6:** Effect of total pressure on the gas product composition working with both oxygen carriers. T = 900°C. (a) NiO21- $\gamma$ Al<sub>2</sub>O<sub>3</sub>, NiO/CH<sub>4</sub> = 3.2, (b) NiO18- $\alpha$ Al<sub>2</sub>O<sub>3</sub>, NiO/CH<sub>4</sub> = 2.2

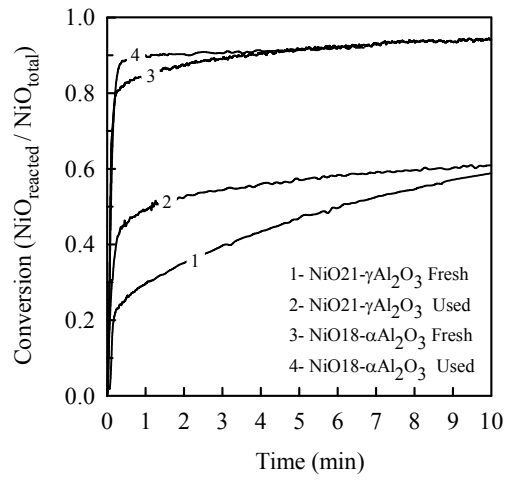


**Figure 7:** Reactivity in TGA of both oxygen carriers.  $T = 900^{\circ}\text{C}$

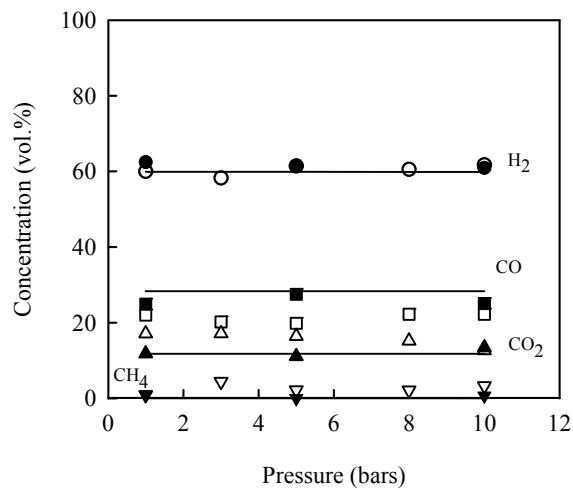


**Figure 8:** Effect of total pressure on the gas product composition for both oxygen carriers.  $T = 900^{\circ}\text{C}$ ,  $\text{NiO}_{\text{reacted}}/\text{CH}_4 = 1.8$ . Filled dots:  $\text{NiO}_{18-\alpha}\text{Al}_2\text{O}_3$ . Empty dots:  $\text{NiO}_{21-\gamma}\text{Al}_2\text{O}_3$ . Lines: thermodynamic equilibrium data.

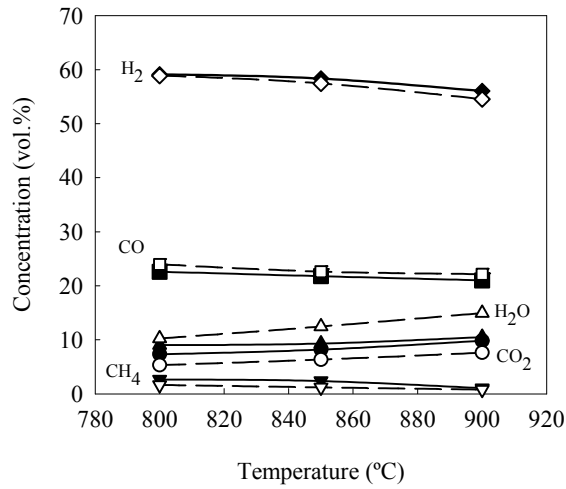


**Figure 9:** Effect of reduction reaction temperature on the gas product composition working with the oxygen carrier NiO18- $\alpha$ Al<sub>2</sub>O<sub>3</sub>. NiO/CH<sub>4</sub> = 1.4. Empty dots: P=1 bar. Filled dots: P = 10 bars.

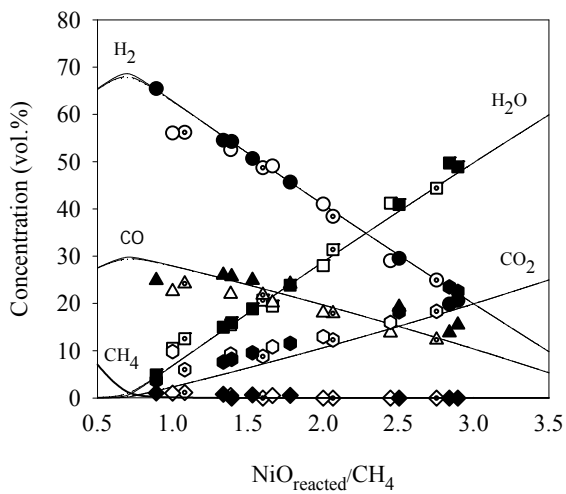


**Figure 10:** Effect of oxygen carrier-to-fuel ratio on the gas product compositions at different operating pressures for the NiO18- $\alpha$ Al<sub>2</sub>O<sub>3</sub> oxygen carrier. T = 900°C. Filled dots: P = 1 bar. Semi-filled dots: P = 5 bars. Empty dots: P = 10 bars. Lines: thermodynamic equilibrium data.

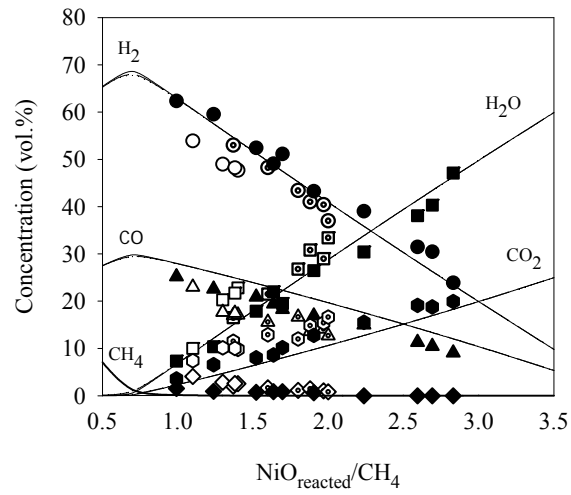


**Figure 11:** Effect of oxygen carrier-to-fuel ratio on the gas product concentrations at different operating pressures for the NiO<sub>21</sub>- $\gamma$ -Al<sub>2</sub>O<sub>3</sub> oxygen carrier. T = 900°C. Filled dots: P = 1 bar. Semi-filled dots: P = 5 bars. Empty dots: P = 10 bars. Lines: thermodynamic equilibrium data.

a)

b)

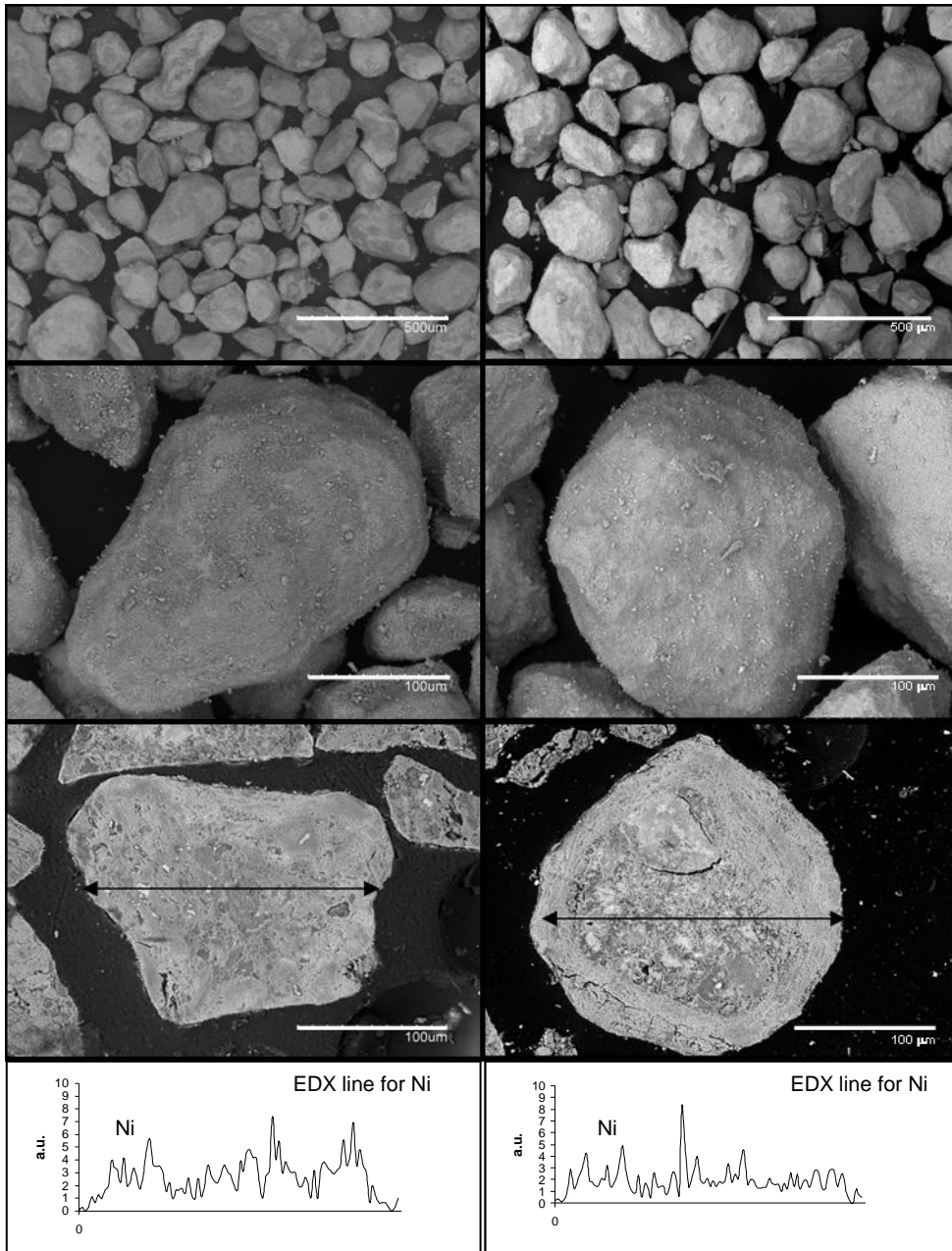


**Figure 12:** SEM images of the NiO18- $\alpha$ Al<sub>2</sub>O<sub>3</sub> oxygen carrier, (a) fresh particles, (b) used particles, and EDX analysis for Ni distribution in the cross section of the particle.



## Captions for the Figures

**Figure 1:** Chemical-Looping Reforming.

**Figure 2:** Thermodynamic equilibrium gas composition for different operating pressures and temperatures.

**Figure 3:** Schematic diagram of the semicontinuous pressurized fluidized bed facility for CLRa

**Figure 4:** H<sub>2</sub>O concentration in the gas outlet stream before and after installation of the furnace around the solid feed hopper. Fluidizing gas: N<sub>2</sub>. T = 900°C

**Figure 5:** Typical reduction test in the semicontinuous fluidized bed facility.

NiO<sub>21</sub>- $\gamma$ Al<sub>2</sub>O<sub>3</sub>, P = 5 bars, T = 900°C

**Figure 6:** Effect of total pressure on the gas product composition working with both oxygen carriers. T = 900°C. (a) NiO<sub>21</sub>- $\gamma$ Al<sub>2</sub>O<sub>3</sub>, NiO/CH<sub>4</sub> = 3.2, (b) NiO<sub>18</sub>- $\alpha$ Al<sub>2</sub>O<sub>3</sub>, NiO/CH<sub>4</sub> = 2.2

**Figure 7:** Reactivity in TGA of both oxygen carriers. T = 900°C

**Figure 8:** Effect of total pressure on the gas product composition for both oxygen carriers. T = 900°C, NiO<sub>reacted</sub>/CH<sub>4</sub> = 1.8. Filled dots: NiO<sub>18</sub>- $\alpha$ Al<sub>2</sub>O<sub>3</sub>. Empty dots: NiO<sub>21</sub>- $\gamma$ Al<sub>2</sub>O<sub>3</sub>. Lines: thermodynamic equilibrium data.

**Figure 9:** Effect of reduction reaction temperature on the gas product composition working with the oxygen carrier NiO<sub>18</sub>- $\alpha$ Al<sub>2</sub>O<sub>3</sub>. NiO/CH<sub>4</sub> = 1.4. Empty dots: P = 1 bar. Filled dots: P = 10 bars.

**Figure 10:** Effect of oxygen carrier-to-fuel ratio on the gas product compositions at different operating pressures for the NiO<sub>18</sub>- $\alpha$ Al<sub>2</sub>O<sub>3</sub> oxygen carrier. T = 900°C. Filled

dots: P = 1 bar. Semi-filled dots: P = 5 bars. Empty dots: P = 10 bars. Lines:  
thermodynamic equilibrium data.

**Figure 11:** Effect of oxygen carrier-to-fuel ratio on the gas product concentrations at different operating pressures for the NiO<sub>2</sub>1- $\gamma$ Al<sub>2</sub>O<sub>3</sub> oxygen carrier. T = 900°C. Filled dots: P = 1 bar. Semi-filled dots: P = 5 bars. Empty dots: P = 10 bars. Lines: thermodynamic equilibrium data.

**Figure 12:** SEM images of the NiO<sub>18</sub>- $\alpha$ Al<sub>2</sub>O<sub>3</sub> oxygen carrier, (a) fresh particles, (b) used particles, and EDX analysis for Ni distribution in the cross section of the particle

**Table 1.** CH<sub>4</sub> concentrations at different total pressures for a constant CH<sub>4</sub> partial pressure

Total Pressure (bars)	1	3	5	8	10
CH <sub>4</sub> (vol. %)	50	16.7	10	6.25	5

**Table 2.** Physical properties and solid composition of the oxygen carriers

Oxygen carrier	Density (g/cm <sup>3</sup> )	Crushing strength (N)	BET (m <sup>2</sup> /g)	Porosity (%)	XRD
NiO21- $\gamma$ -Al <sub>2</sub> O <sub>3</sub> Fresh	1.7	2.6	83.4	50.7	$\gamma$ -Al <sub>2</sub> O <sub>3</sub> , NiAl <sub>2</sub> O <sub>4</sub>
NiO21- $\gamma$ -Al <sub>2</sub> O <sub>3</sub> Used	1.8	2.4	29.5	50.6	$\gamma$ -Al <sub>2</sub> O <sub>3</sub> , NiAl <sub>2</sub> O <sub>4</sub>
NiO18- $\alpha$ -Al <sub>2</sub> O <sub>3</sub> Fresh	2.4	4.1	7.0	42.5	$\alpha$ -Al <sub>2</sub> O <sub>3</sub> , NiO, NiAl <sub>2</sub> O <sub>4</sub>
NiO18- $\alpha$ -Al <sub>2</sub> O <sub>3</sub> Used	2.5	4.0	7.7	42.1	$\alpha$ -Al <sub>2</sub> O <sub>3</sub> , NiO, NiAl <sub>2</sub> O <sub>4</sub>